



# Characterization and corrosion protection of nano-titanium dioxide doped BTSE-GPTMS sol–gel coating on cast Al–Si alloy

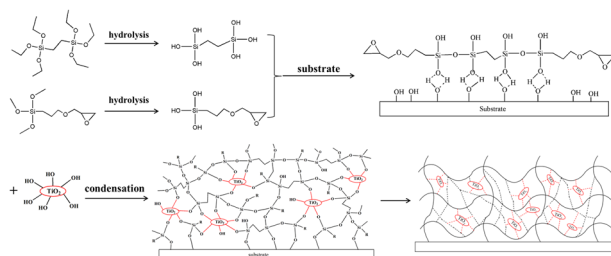
Xuelin Huang<sup>1,2</sup> · Rui Ke<sup>1,2</sup> · Yinsheng Dong<sup>2</sup>

Received: 12 June 2019 / Accepted: 18 December 2019 / Published online: 8 January 2020  
© Springer Science+Business Media, LLC, part of Springer Nature 2020

## Abstract

A hybrid organic–inorganic sol–gel coating was prepared on the surface of cast aluminum–silicon (Al–Si) alloy via dip coating method to improve the anticorrosion ability. In the present work, bis(triethoxysilyl) ethane (BTSE) and 3-glycidoxypropyl-trimethoxysilane (GPTMS) were employed as the precursors to prepare hybrid sol–gel (BG) coating. Nano titanium dioxide (nano-TiO<sub>2</sub>) was introduced to improve the corrosion resistance of the coating. The microstructures of the BG/nano-TiO<sub>2</sub> (BG-T) coating was characterized by scanning electron microscopy (SEM), energy dispersive spectrometer (EDS), and Fourier-transform infrared (FT-IR) spectroscopy. The results showed that there was a chemical reaction between nano-TiO<sub>2</sub> and BG coating and a complete defect-free coating formed on the surface of Al–Si alloy. Moreover, there were a few only minor cracks appeared on the surface of BG-T coating after 15 days immersion in 3.5 wt.% NaCl solution. The corrosion resistant performances of the coatings were evaluated by the electrochemical tests. The results showed that the nano-TiO<sub>2</sub> particles elevated the corrosion potential and depressed the corrosion current, thereby improved the corrosion resistance. The long-term immersion tests of BG and BG-T coating further showed that the BG-T coating possesses an excellent long-term stability for corrosion protection.

## Graphical Abstract



## Highlights

- Nano-TiO<sub>2</sub> doped sol-gel coating was applied in simple and direct way over cast Al-Si alloy.
- Nano-TiO<sub>2</sub> doped sol-gel coating enhanced the cast Al-Si alloy corrosion resistance protection ability than undoped one.
- The corrosion resistance of the BG-T coating was revealed by electrochemical, SEM and EDS studies.
- Reaction mechanism of nanoparticles with sol-gel was studied.

**Keywords** Corrosion resistance · Sol–gel · Hybrid coating · Cast Al–Si alloy

✉ Yinsheng Dong  
dongys@seu.edu.cn

<sup>1</sup> School of Materials Science and Engineering, Southeast

University, Nanjing 211189, China

<sup>2</sup> Jiangsu Key Laboratory of Advanced Metallic Materials,  
Nanjing 211189, China

## 1 Introduction

Cast aluminum–silicon (Al–Si) alloy is widely used in automobile, ship, aerospace, and other fields due to their light weight, high intensity, good casting forming, and employing performance [1–3]. However, a previous study identified many Fe, Cu, Mg, and Mn intermetallic phases in cast Al–Si alloys [4–6]. The presence of alloying elements make the alloy susceptible to localized corrosion, such as pitting corrosion, intergranular corrosion, and stress corrosion cracking [7, 8]. Therefore, it is necessary to improve the surface properties of the cast Al–Si alloy in order to enhance the corrosion resistance. The conventional methods of the Al alloy corrosion protection are usually chromate treatments and chromate-containing coatings [9, 10]. Unfortunately, the hexavalent chromate compounds are toxic and could cause a lot of damage to our health and environment [11–13]. Therefore, it is highly desired to develop alternative protective coatings to replace the chromate coating for corrosion protection of Al alloys. In the past decades, various surface treatment techniques [14–19] have been developed to enhance the corrosion resistance of Al alloys, such as phosphate salts coating, sol–gel techniques, cerium-impregnated coatings, and so on.

Sol–gel coating is regarded as one of the most promising treatments for Al alloys among the various protective coatings. On the one hand, sol–gel coating is able to establish chemical bonds with the substrate surface, thereby offering good adhesion ability [20]. On the other hand, sol–gel coating can form an inactive barrier coating on the substrate surface, thus improving the corrosion property of the material [21, 22]. Moreover, the organic–inorganic hybrid sol–gel coatings [23, 24] is not only providing good mechanical properties but also improving the flexibility and ductility. Li et al. [25] prepared an anticorrosion coating of the inorganic–organic hybrid coatings (HC) for the protection of Al alloy by a dipping and room temperature curing method. Mrad et al. [26] investigated the dependence of the anticorrosion performance of a poly ( $\gamma$ -GPTMS) sol–gel coating on AA2024-T3 aluminum alloy surface with different preparation method. All the test results show that the sol–gel coating is applied on the aluminum alloy surfaces pretreated by chemical etching exhibit a good anticorrosion performance. Moreover, many studies show that the introduction of inorganic nanoparticles could effectively improve the mechanical properties and corrosion resistance of sol–gel coating [20, 27]. The introduction of inorganic nanoparticles can increase the crosslinking degree of the coating and improve the densification of hybrid sol–gel coatings, which results in that the coating achieves a good anticorrosion performance. Yu et al. [28] prepared a hybrid titania-containing sol–gel coating, the coating has been modified through additions of different pigments (contain a

copolymer polyvinyl butyral, a conductive polymer poly-aniline and a corrosion resistant glass flake) to investigate the influence of these pigments for the corrosion protection of AA2024-T3 alloy. The physical, chemical, and corrosion properties of the modified coatings were also studied. Peres et al. [29] investigated the anticorrosion performance of TEOS-GPTMS HCs on AZ31 alloy with the addition of different content of SiO<sub>2</sub> nanoparticles, which showed that the addition of the nanoparticles could improve the corrosion resistance of the coating. Besides those mentioned above, TiO<sub>2</sub> has photocatalytic activity and can prevent bacteria from damaging the substrate and coating by killing bacteria [30, 31]. Meanwhile, TiO<sub>2</sub> produces a large number of electrons under ultraviolet light, which may inhibit the corrosion of metals and in some degree achieve photocathode protection [32, 33].

Herein, the corrosion resistance coating was successfully fabricated on the cast Al–Si alloy surface by dip coating method. In this system, the introduction of nano-TiO<sub>2</sub> could help to improve the densification and achieve a good barrier property of the BTSE-GPTMS hybrid sol–gel/nano-TiO<sub>2</sub> (BG-T) coating. The chemical structure was analyzed by Fourier-transform infrared (FT-IR). The coatings morphology and microstructure were observed by scanning electron microscopy (SEM) and their compositions were analyzed by energy dispersive spectrometer (EDS). Meanwhile, the corrosion resistance and long-term durable performances of the coatings were evaluated by electrochemical impedance spectroscopy (EIS) and potentiodynamic polarization. The mechanism of nano-TiO<sub>2</sub> modification was also discussed in detail. The as-prepared BG-T coating was certified to have a long-term durable performance and can be prolongs its service life.

## 2 Experimental

### 2.1 Materials and chemicals

Samples of cast Al–Si (EN AC-43000) alloy with dimensions of 15 × 15 × 3 mm were used as the substrate material. The chemical composition of the alloy is listed in Table 1. The substrates were abraded with emery abrasive papers from 200 to 1000 grits and washed with deionized water. Then the substrates were immersed in alkali solution (including 5 wt.%

**Table 1** Chemical composition of the received material

Element	Si	Mg	Fe	Ni
wt. %	9.850%	0.225%	0.122%	0.004%
Element	Ti	Mn	Zn	Al
wt. %	0.024%	0.136%	0.070%	89.50%

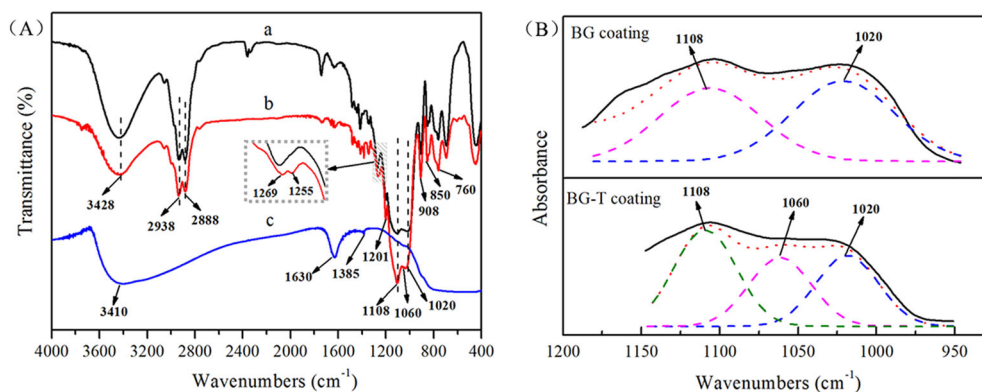


**Fig. 1** FT-IR spectra and fitting analysis of (a) BG coating, (b) BG-T coating, and (c) nano-TiO<sub>2</sub>

sodium hydroxide and 3.5 wt.% sodium carbonate) at room temperature for 1 min. Afterwards, the substrates were ultrasonically cleaned with deionized water and anhydrous ethanol for 3 min at room temperature, respectively, and kept dry prior to use. Bis (triethoxysilyl) ethane (BTSE) and 3-glycidoxypropyl-trimethoxysilane (GPTMS) were purchased from Bide Pharmatech Ltd. Nano-TiO<sub>2</sub> (99.8%, 5–10 nm, anatase) was purchased from Aladdin. All chemicals were used without further purification. Self-made deionized water was used in the experiment process.

## 2.2 Synthesis and characterization of hybrid sol-gel coating

The coating solution (coating I) was prepared from precursors of GPTMS and BTSE. In detail, GPTMS (12 mL) and BTSE (10 mL) were added in turn to mixed solution of water (10 mL) and ethanol (100 mL). Afterwards, 0.5 mL acetic acid was added as catalyst to ensure hydrolysis reaction. The mixed solution was stirred at room temperature for 12 h. Finally, the final coating solution was obtained. The second coating solution (coating II) was prepared by adding nano-TiO<sub>2</sub> (1.6 g) into 100 mL coating I solution, followed by high speed stirring 1 h at room temperature. The final molar ratio of coating solution II was GPTMS: BTSE: nano-TiO<sub>2</sub> = 2:1:1. The surface coating was fabricated by immersing the cleaned alloy substrate in the coating solution II, withdrawing from the solution at a speed of 10 cm/min. Subsequently, the treated substrate was dried for 30 min at 120 °C and the BG-T coating was obtained. In a comparison, the BG coating without introduction of nano-TiO<sub>2</sub> was also prepared by similar process.

## 2.3 Characterization

The chemical composition and structure of the BG and BG-T coatings were characterized by FT-IR spectrophotometer (Nicolet iS10, U.S. Company Thermo Scientific) within a

range of 400–4000 cm<sup>-1</sup>, the resolution is 4 and the number of sample scans is 16. The coatings were scraped from the substrate and prepared as a finely pressed powder. The coating powder and KBr are mixed and pressed for infrared transmission spectra. The morphologies and elemental analysis of the Al-Si alloy, BG, and BG-T coating were investigated by SEM (Sirion) equipped with an EDS. The potentiodynamic polarization analyses and EIS were used for analyzing the corrosion resistant performances of the samples in 3.5 wt.% NaCl aqueous solution, which was carried out with a CHI604E electrochemical workstation (Shanghai Chenhua Instruments Inc., PR China). A three-electrode cell was used: a working electrode (the sample with an exposed area of 1 cm<sup>2</sup>), a platinum sheet counter electrode and a saturated calomel reference electrode (SCE). After 1 h of initial delay, the polarization curves were scanned from -1.5 V to 0.5 V at a rate of 0.01 V/s. The measuring frequency range of the EIS test was from 100 kHz down to 100 mHz with a perturbation potential of 0.02 V.

## 3 Results and discussions

### 3.1 FT-IR spectra of samples

Figure 1 shows the FT-IR spectra of BG coating, BG-T coating and nano-TiO<sub>2</sub>. The peaks at 3410, 1630, 1385 cm<sup>-1</sup> and range from 400 to 700 cm<sup>-1</sup> shown in Fig. 1c are characteristics of nano-TiO<sub>2</sub> [34, 35]. Remarkably, there is a peak located at 3410 cm<sup>-1</sup> corresponding to the characteristic absorption peak of hydroxyl group, which confirm the existence of hydroxyl groups on the surface of nano-TiO<sub>2</sub>. Form the profile of the BG coating as shown in Fig. 1a, the peaks appeared at wave number 3428 and 760 cm<sup>-1</sup> correspond to stretching vibration of functional groups of -O-H and the Si-O, respectively. The peaks at wave numbers 2938 and 2888 cm<sup>-1</sup> are belong to the C-H stretching vibration absorption and the peaks at 1269 and 908 cm<sup>-1</sup> are assigned

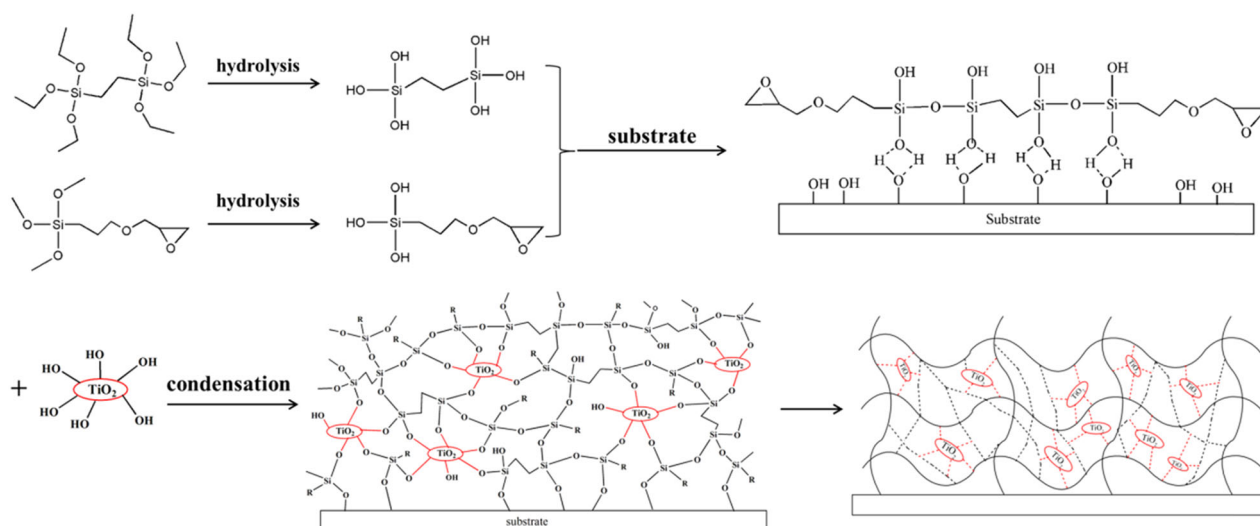


**Fig. 2** Schematic illustration for the reaction of BTSE, GPTMS, and nano-TiO<sub>2</sub>

to the characteristic absorption peak of epoxy group [24]. The relative bands at around 1020 and 1108  $\text{cm}^{-1}$  are related to the stretching vibration of the Si–O–Si chemical bond [25, 26, 36], which indicate the successful condensation process. Compared with the profile of BG coating, the peak area of hydroxyl group (the peak at 3428  $\text{cm}^{-1}$ ) is obviously reduced on the spectra of BG-T coating as shown in Fig. 1b. Besides, according to the fitting analysis of FT-IR in Fig. 1b, an obvious peak of BG-T coating appears at 1060  $\text{cm}^{-1}$ , which is associated with the Si–O–Ti stretching vibration [37, 38]. Test results show that nano-TiO<sub>2</sub> and BG sol–gel are bonded together through a chemical reaction.

Figure 2 shows the mechanism model of the BG-T coating preparation process. Above all, BTSE and GPTMS react with water to form Si–OH by hydrolysis reaction under acetic acid catalysis. Afterwards, the Si–OH groups form oligomeric siloxane through the dehydration condensation reaction, and a three-dimensional cross-linked network structure is formed after a curing reaction. Moreover, the above mentioned Si–OH and hydroxyl groups of the substrate produced by the alkali treatment [26] could form strong Si–O–Al covalent bond on the surface of Al–Si alloys under a curing reaction [15, 39]. Besides, the FT-IR results imply the existence of hydroxyl group on the surface of the nano-TiO<sub>2</sub>, which can react with Si–OH to form Ti–O–Si covalent bonds [37]. These results could confirm an improved density of the cross-linked network in this system that can increase the shielding effectiveness, and thus improve the corrosion resistance of the coating.

### 3.2 Morphologies of samples

The morphologies of Al–Si alloy, BG, and BG-T coatings are observed by SEM and the images are shown in Fig.

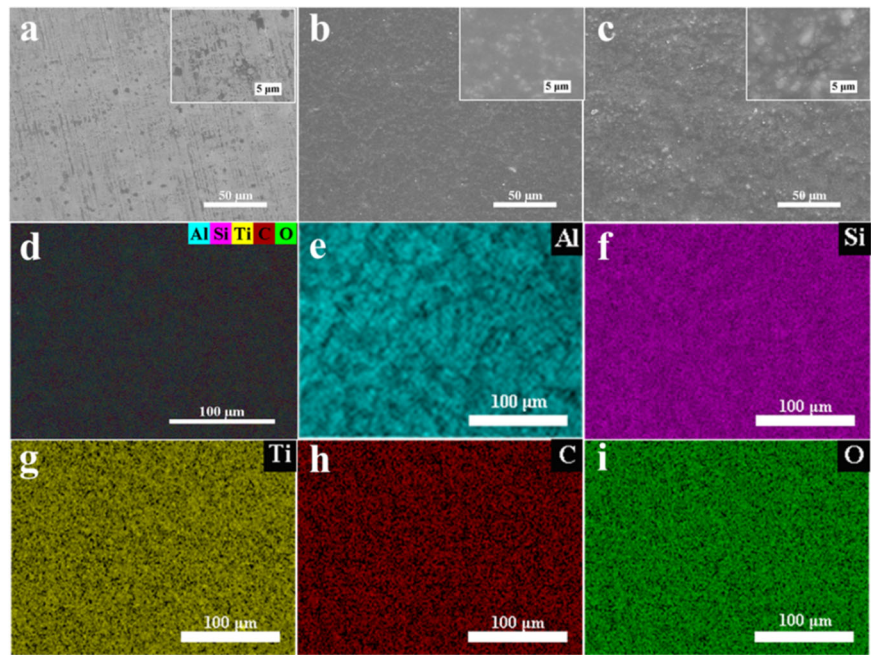
3a–c. Figure 3a shows the typical micromorphology of Al–Si alloy, there are a multitude gray spots of silicon particle on the surface of substrate [40–42]. The BG coating covers the substrate surface uniformly and there are no cracks and holes observed as shown in Fig. 3b. The microstructure of the BG-T coating is similar to that of BG coating, while many island particles can be discovered from the high-resolution image as shown in Fig. 3c. Figure 3d–i presents the EDS mapping images for the distribution of the elements in BG-T coating (Fig. 3c). It can be seen that all elements in the BG-T coating, especially Ti element, have uniform distribution, indicating a uniform, and compact coating on the Al–Si alloy substrate.

Figure 4 shows the SEM images for the cross-section of the BG and BG-T coatings, and the corresponding elemental mapping of the BG-T coating. As can be seen in the Fig. 4a, a', the thickness of BG coating is about  $2.7 \pm 0.3 \mu\text{m}$ . Moreover, there is no crack and pore defect on the coating and high bond strength exists between the coating and substrate. In addition, the thickness of BG-T coating is about  $3.0 \pm 0.3 \mu\text{m}$  and the cross-section micrographs is similar to that of the BG coating shown in the Fig. 4b, b'. It can be deduced that introducing nano-TiO<sub>2</sub> into the BG coating will not destroy the original microstructure of the coating and only shows an increase in thickness slightly.

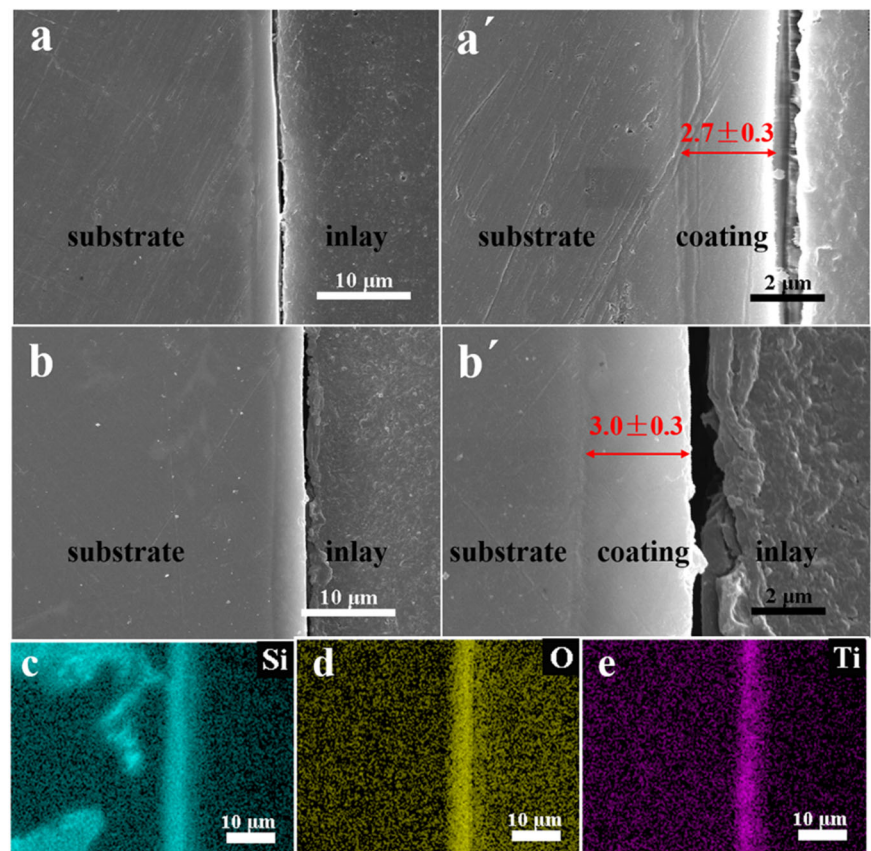
### 3.3 Morphologies of the samples with different immersion time

In addition, immersion corrosion tests are performed to investigate the corrosion resistance of the samples. Figure 5 shows the SEM images of the Al–Si alloy, BG, and BG-T coating after 7 and 15 days immersion in 3.5 wt.% NaCl aqueous solution, respectively. For the Al–Si alloy, serious

**Fig. 3** a–c surface morphologies with different magnification of Al–Si alloy, BG, and BG-T coating, respectively. d–i the elemental mapping of the BG-T coating (c)



**Fig. 4** Cross-section micrographs (a, a') with different magnification of BG coating. Cross-section micrographs (b, b') with different magnification of BG-T coating and the corresponding elemental mapping (c–e)



pitting corrosion on the surface of the substrate was occurred after 7 days of immersion and it was completely destroyed after 15 days. For the BG coating, it showed a lot of cracks on the surface of the coating after 7 days

immersion. The cracks on the coating surface became larger from 1.8 to 10.8 μm in the width after 15 days. For the BG-T coating, the morphology of the coating is similar to that of the original sample (Fig. 3c). In addition, the surface of the

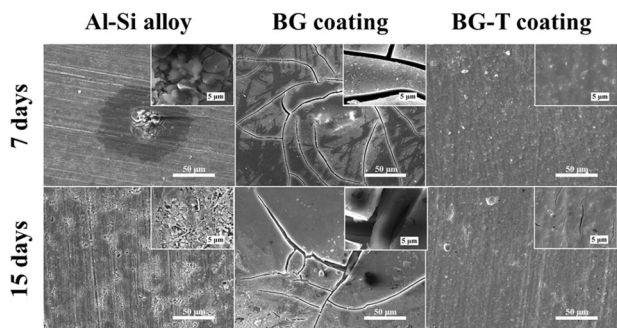


**Fig. 5** Surface morphologies with different immersion time of Al–Si alloy, BG, and BG-T coating

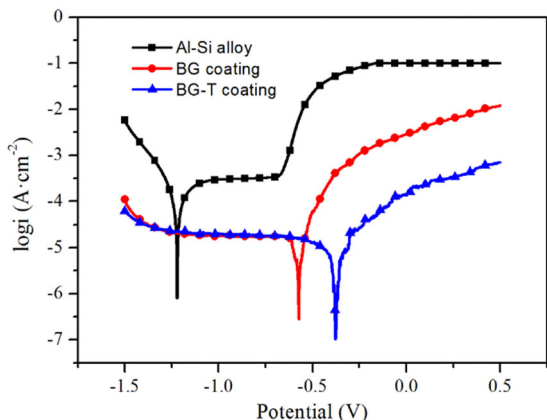


**Fig. 6** The potentiodynamic polarization plots of Al–Si alloy, BG, and BG-T coating

coating did not significantly change after 7 days immersion. Until immersion for 15 days, small cracks appeared on the surface of the coating, which was about 0.4 μm in the width. The results show that the corrosion resistance of BG-T coating is better than that of BG coating. It can be deduced that a dense coating with a network structure is formed by introduction of nano-TiO<sub>2</sub>, which makes the coating more stable in the external environment.

**3.4 Corrosion resistance of coatings**

The polarization curves and electrochemical parameters of the Al–Si alloy, BG, and BG-T coating after immersion of 1 h in 3.5% NaCl aqueous solution are shown in Fig. 6 and resulting data are exhibited in Table 2, respectively. The corrosion potential (*E*<sub>corr</sub>) and corrosion current density (*I*<sub>corr</sub>) are calculated from the plots by extrapolation method [43, 44]. Besides, the protection efficiency *η* is calculated by the following equation [45–47]:

$$\eta \% = \frac{(I_{\text{corr}}^0 - I_{\text{corr}}^1)}{I_{\text{corr}}^0} \times 100\%$$

**Table 2** The electrochemical parameters of the samples

Sample	<i>E</i> <sub>corr</sub> (V SCE)	<i>I</i> <sub>corr</sub> (A cm <sup>2</sup> )	<i>η</i>
Al–Si alloy	−1.22	1.66 × 10 <sup>−4</sup>	–
BG coating	−0.58	1.10 × 10 <sup>−5</sup>	93.37
BG-T coating	−0.38	6.03 × 10 <sup>−6</sup>	96.37

where *I*<sub>corr</sub><sup>0</sup> and *I*<sub>corr</sub><sup>1</sup> are the corrosion current density of the bare substrate and coated samples, respectively. Compared with untreated substrate, the *E*<sub>corr</sub> value of BG coating is positive about 700 mV, while the *I*<sub>corr</sub> value is about 1.10 × 10<sup>−5</sup> A cm<sup>2</sup>, which decreases with about one order of magnitude. Thus, the corrosion resistant property of Al–Si alloy is improved effectively by BG coating, which is due to the BG coating acts as a physical barrier to block the aggressive media from attacking the surface of the substrate [25, 48]. Moreover, the curve of BG-T coating is similar to that of the BG coating. Whereas the *E*<sub>corr</sub> is more positive than that of BG coating, while the *I*<sub>corr</sub> is about 6.03 × 10<sup>−6</sup> A cm<sup>2</sup> and much lower than that of the BG coating. More importantly, the *η* of the BG-T coating calculated is 96.37%, significantly higher than 93.37% of BG coating. The results show that the addition of nano-TiO<sub>2</sub> can effectively improve the corrosion resistance of the coating.

As an effective and powerful measurement, the EIS is used to evaluate the barrier and anticorrosion capability of different coatings in 3.5 wt.% NaCl solution. Figure 7 shows the Nyquist plots of the different coating systems. The capacitive loop of the BG and BG-T coatings are significantly higher than the untreated substrate, which further indicates that the coating can effectively improve the corrosion resistance of the substrate. Moreover, compared with the capacitive loop of the BG coating, the diameter of the capacitive loop of the BG-T coating increases significantly, which indicates that the BG-T coating can enhance the corrosion resistance more effectively than BG coating. Besides, with the extension of immersion time, the Nyquist plots show the shrinking capacitive loop, implying the declined corrosion protective performance of the substrate [23, 45].

The bode plots and bode phase of the bare substrate, BG and BG-T coating during immersion in 3.5% NaCl are shown in Fig. 8. The corresponding equivalent circuit (EC) models for the EIS spectra are presented in Fig. 9. The Fitted results are listed in Tables 3–5. For the bode plots, the impedance modulus at low frequency (*|Z|* 0.1 Hz) is used to measure the ability of coating to prevent corrosion [49]. As a general rule, a larger *|Z|* in low frequency indicates a better corrosion resistance. The values of the impedance modulus (*|Z|* 0.1 Hz) of the coatings are larger than that of the bare substrate, and the BG-T coating has the largest values. As revealed by the phase angle plots, the bare substrate seemed

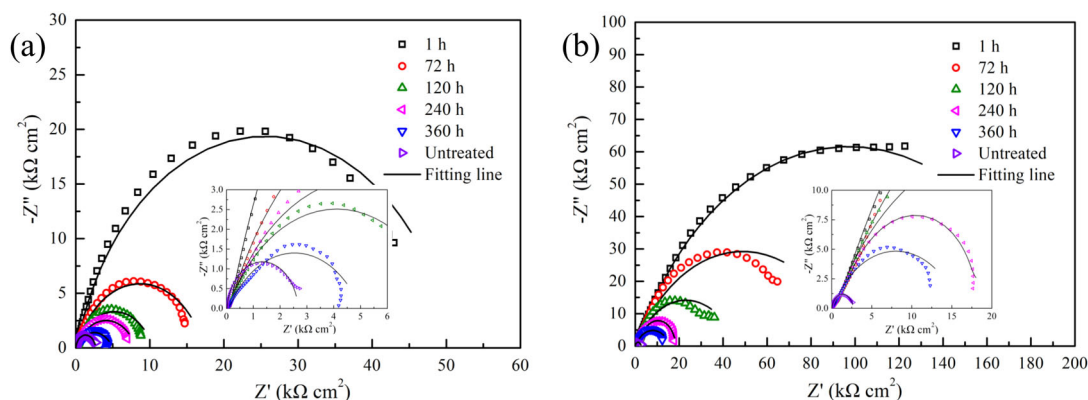


**Fig. 7** The Nyquist plots of bare substrate, BG coating (a) and BG-T coating (b)

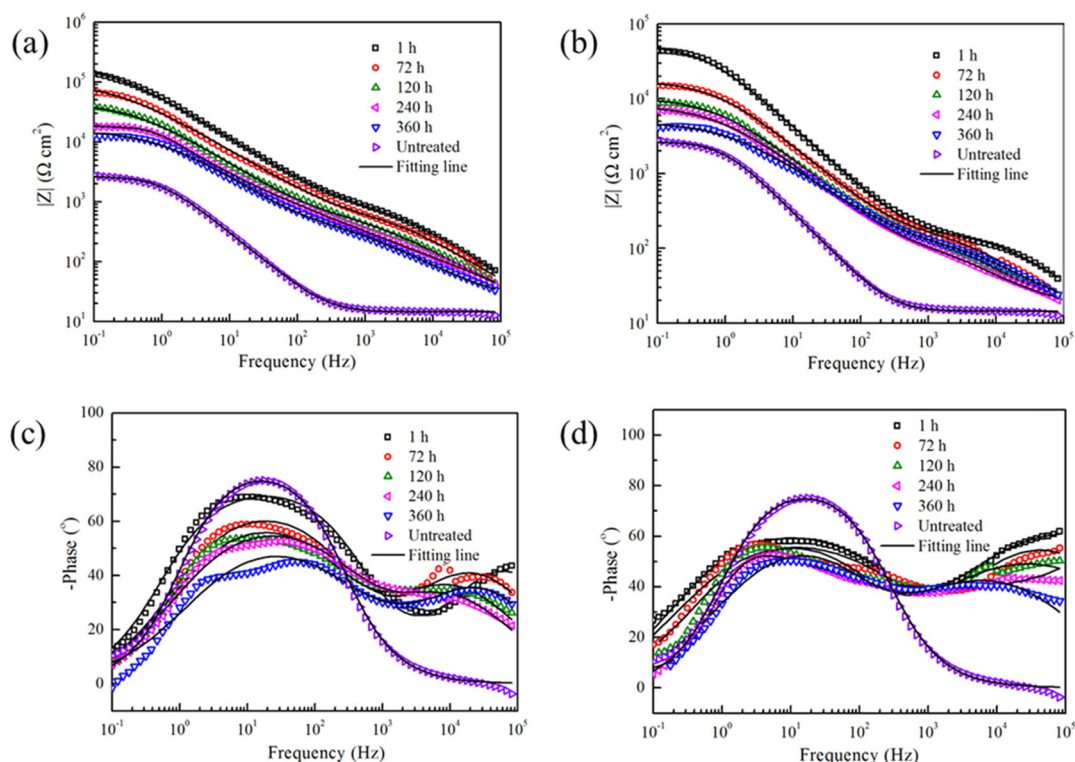


**Fig. 8** EIS Bode plots obtained for the bare substrate and coating samples with different immersion time. **a** Bode impedance of BG coating, **b** bode impedance of BG-T coating, **c** bode phase of BG coating, and **d** bode phase of BG-T coating

to have one time constant over the recorded range, the EC1 in Fig. 9 can be used to fitting the EIS result of the bare substrate. In contrast, the BG and BG-T coating samples show mainly two-time constants and an EC2 model can be used to describe their behavior. Where  $R_s$  is the solution resistance,  $R_p$  and  $Q_p$  present the coating resistance and capacitance.  $R_{ct}$  and  $Q_{ct}$  represent the charge-transfer resistance and double-layer capacitance, which is used to describe the charge-transfer process of the interface of the coating. The CPE is used to replace the coating capacitance due to the electric double-layer cannot act as an ideal

capacitor in real electrochemical system. The barrier layer resistance (approximate to the  $R_{ct}$ ) of each sample is obtained from the fitting results. It can also be seen from Fig. 10 and Tables 3–5 that the  $R_{ct}$  of BG coating is decreased from 50.9 to 4.9 k $\Omega$  cm $^2$  with the immersion time increasing, the final value is slightly higher than that of the original substrate. However, the introduction of nano-TiO $_2$  could effectively improve both the normal and prolonged anticorrosion performance, and the  $R_{ct}$  could reach 193 k $\Omega$  cm $^2$  at the initial immersion, which is significantly higher than that of the BG coating. Besides, the decreasing speed

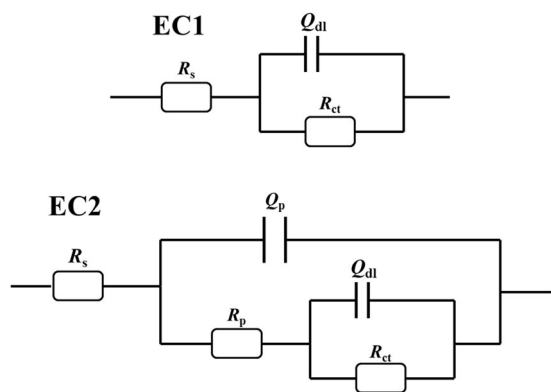


**Fig. 9** Equivalent circuits (EC) used to fit the EIS diagrams for (a) bare substrate, (b) BG and BG-T coating

**Table 3** EIS fitting parameters of the Al–Si alloy

Samples	$R_s$ $\Omega\text{ cm}^2$	$Q_p$ $S^n\ \Omega^{-1}\text{ cm}^{-2}$	$R_{ct}$ $\Omega\text{ cm}^2$
Al–Si alloy	14.36	$7.10 \times 10^{-5}$	$2.67 \times 10^3$

**Table 4** EIS fitting parameters of the BG coating systems at various immersion times

Samples	$R_s$ $\Omega\text{ cm}^2$	$Q_p$ $S^n\ \Omega^{-1}\text{ cm}^{-2}$	$R_p$ $\Omega\text{ cm}^2$	$Q_{ct}$ $S^n\ \Omega^{-1}\text{ cm}^{-2}$	$R_{ct}$ $\Omega\text{ cm}^2$
1 h	13.74	$1.17 \times 10^{-6}$	$1.49 \times 10^2$	$6.36 \times 10^{-6}$	$5.09 \times 10^4$
72 h	13.15	$4.82 \times 10^{-6}$	$1.83 \times 10^2$	$1.30 \times 10^{-5}$	$1.71 \times 10^4$
120 h	15.73	$1.07 \times 10^{-5}$	$1.64 \times 10^2$	$2.03 \times 10^{-5}$	$1.02 \times 10^4$
240 h	16.02	$2.52 \times 10^{-5}$	$1.17 \times 10^2$	$2.52 \times 10^{-5}$	$8.03 \times 10^3$
360 h	14.17	$5.36 \times 10^{-6}$	$1.14 \times 10^2$	$4.52 \times 10^{-5}$	$4.86 \times 10^3$

**Table 5** EIS fitting parameters of the BG-T coating systems at various immersion times

Samples	$R_s$ $\Omega\text{ cm}^2$	$Q_p$ $S^n\ \Omega^{-1}\text{ cm}^{-2}$	$R_p$ $\Omega\text{ cm}^2$	$Q_{ct}$ $S^n\ \Omega^{-1}\text{ cm}^{-2}$	$R_{ct}$ $\Omega\text{ cm}^2$
1 h	19.37	$9.63 \times 10^{-7}$	$1.11 \times 10^3$	$3.39 \times 10^{-6}$	$1.93 \times 10^5$
72 h	10.93	$1.03 \times 10^{-6}$	$6.63 \times 10^2$	$6.84 \times 10^{-6}$	$9.68 \times 10^4$
120 h	19.78	$5.03 \times 10^{-6}$	$8.15 \times 10^2$	$6.96 \times 10^{-6}$	$4.52 \times 10^4$
240 h	15.79	$1.09 \times 10^{-5}$	$3.27 \times 10^3$	$8.31 \times 10^{-5}$	$3.77 \times 10^4$
360 h	17.88	$1.17 \times 10^{-5}$	$6.35 \times 10^2$	$9.11 \times 10^{-6}$	$1.54 \times 10^4$

of  $R_{ct}$  of BG-T coatings is obviously less than that of BG coatings during the immersion period. This is because the existed nano-TiO<sub>2</sub> improves the density of the coating, which increases the shielding effectiveness and retards the degradation of the coating in chloride solution [50]. Even after immersion for 360 h, the  $R_{ct}$  also still keep as large as 15.4 kΩ cm<sup>2</sup>, which is approximately three times higher than that of the bare substrate. These test results show that doped nano-TiO<sub>2</sub> coating could significantly enhance the

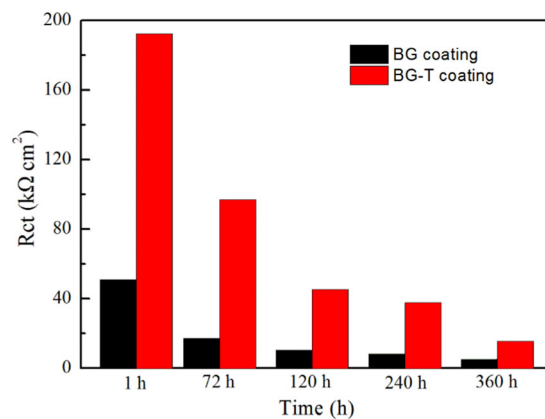


**Fig. 10** Resistance of the BG and BG-T coating with different immersion time

sustainable corrosion protection performance of the Al–Si alloy substrate.

### 4 Conclusion

In summary, hybrid organic–inorganic sol–gel coating modified with nano-TiO<sub>2</sub> was successfully fabricated on cast Al–Si alloy substrate with uniform thicknesses by condensation reaction and the nanoparticles distribute uniformly in the organic matrix. The addition of nano-TiO<sub>2</sub> has a significant effect on the structure and performance of the composite coatings. The morphology of the BG-T coating presents that a dense and uniformly covers on the Al–Si alloy substrate formed a corrosion resistance coating and exhibits excellent interfacial adherence with the substrate. Moreover, the BG-T coating shows no significant variation after 7 days of immersion in 3.5 wt.% NaCl solution and only a small number of cracks appeared on the surface after 15 days immersion. The corrosion resistance of the BG coating could be improved effectively by introduction of nano-TiO<sub>2</sub>, which leads to reduce the corrosion current and makes the corrosion potential more positive. Moreover, the impedance modulus value reached above 193 kΩ cm<sup>2</sup>. Notably, after 360 h immersion, the coating still had excellent protective effect.

### Compliance with ethical standards

**Conflict of interest** The authors declare that they have no conflict of interest.

**Ethical approval** This article does not contain any studies with human participants or animals performed by any of the authors.

**Informed consent** Informed consent was obtained from all individual participants included in the study.



**Publisher's note** Springer Nature remains neutral with regard to jurisdictional claims in published maps and institutional affiliations.

## References

- Yu HJ, Dong Q, Chen Y, Chen CZ (2018) Influence of silicon on growth mechanism of micro-arc oxidation coating on cast Al–Si alloy. *R Soc Open Sci* 5:172428–172438
- Dhiman M, Dwivedi DK, Sehgal R, Bhat IK (2008) Effect of iron (wt.%) on adhesive wear response of Al-12Si-1Cu-0.1Mg alloy in dry sliding conditions. *Trans Indian Inst Met* 61:451–456
- Kang N, Coddet P, Liao HL, Baur T, Coddet C (2016) Wear behavior and microstructure of hypereutectic Al–Si alloys prepared by selective laser melting. *Appl Surf Sci* 378:142–149
- Chanyathunyaraj K, Patakham U, Kou S, Limmaneevichitr C (2017) Mechanical properties of squeeze-cast Al-7Si-0.3Mg alloys with sc-modified Fe-rich intermetallic compounds. *Rare Met* 37:769–777
- Patakham U, Limmaneevichitr C (2014) Effects of iron on intermetallic compound formation in scandium modified Al–Si–Mg alloys. *J Alloy Compd* 616:198–207
- Shabestari SG (2004) The effect of iron and manganese on the formation of intermetallic compounds in aluminum-silicon alloys. *Mat Sci Eng A* 383:289–298
- Culliton D, Betts AJ, Kennedy D (2013) Impact of intermetallic precipitates on the tribological and/or corrosion performance of cast aluminium alloys: a short review. *Int J Cast Met Res* 26:65–71
- Mutombo K (2011) Intermetallic particles-induced pitting corrosion in 6061-T651 aluminium alloy. *Mater Sci Forum* 690:389–392
- Zhao J, Xia L, Sehgal A, Lu D, McCreery RL, Frankel GS (2001) Effects of chromate and chromate conversion coatings on corrosion of aluminum alloy 2024-T3. *Surf Coat Technol* 140:51–57
- Grilli R, Baker MA, Castle JE, Dunn B, Watts JF (2011) Corrosion behaviour of a 2219 aluminium alloy treated with a chromate conversion coating exposed to a 3.5% NaCl solution. *Corros Sci* 53:1214–1223
- Wise SS, Holmes AL, Liou L, Adam RM, Wise-Sr JP (2016) Hexavalent chromium induces chromosome instability in human urothelial cells. *Toxicol Appl Pharmacol* 296:54–60
- Blasiak J, Kowalik J (2000) A comparison of the in vitro genotoxicity of tri- and hexavalent chromium. *Mutat Res* 469:135–145
- Ganapathy S, Li P, Lafontant J, Xiong R, Yu TQ, Zhang GJ, Chen CY (2017) Chromium IV exposure, via Src/Ras signaling, promotes cell transformation. *Mol Carcinog* 56:1808–1815
- Chen J, Lan XN, Wang C, Zhang QY (2018) The formation mechanism and corrosion resistance of a composite phosphate conversion film on AM60 alloy. *Materials* 11:402–412
- Vignesh RB, Balaji J, Sethuraman MG (2017) Surface modification, characterization and corrosion protection of 1,3-diphenylthiourea doped sol–gel coating on aluminium. *Prog Org Coat* 111:112–123
- Calado LM, Taryba MG, Carmezim MJ, Montemor MF (2018) Self-healing ceria-modified coating for corrosion protection of AZ31 magnesium alloy. *Corros Sci* 142:12–21
- Pan XM, Wu JS, Ge YZ, Xiao K, Luo H, Gao SJ, Li XG (2014) Preparation and characterization of anticorrosion ormosil sol–gel coatings for aluminum alloy. *J Sol–gel Sci Technol* 72:8–20
- Zhang F, Ju PF, Pan MQ, Zhang DW, Huang Y, Li GL, Li XG (2018) Self-healing mechanisms in smart protective coatings: a review. *Corros Sci* 144:74–88
- Eslami M, Fedel M, Speranza G, Deflorian F, Andersson N-E, Zanella C (2017) Study of selective deposition mechanism of cerium-based conversion coating on Rheo-HPDC aluminium-silicon alloys. *Electrochim Acta* 255:449–462
- Gao X, Yan R, Xu L, Ma HY (2018) Effect of amorphous phytic acid nanoparticles on the corrosion mitigation performance and stability of sol–gel coatings on cold-rolled steel substrates. *J Alloy Compd* 747:747–754
- Maia F, Yasakau KA, Carneiro J, Kallip S, Tedim J, Henriques T, Cabral A, Venâncio J, Zheludkevich ML, Ferreira MGS (2016) Corrosion protection of AA2024 by sol–gel coatings modified with MBT-loaded polyurea microcapsules. *Chem Eng J* 283:1108–1117
- Zheng SX, Li JH (2010) Inorganic-organic sol gel hybrid coatings for corrosion protection of metals. *J Sol–gel Sci Technol* 54:174–187
- Hu JY, Li Q, Zhong XK, Kang W (2008) Novel anti-corrosion silicon dioxide coating prepared by sol–gel method for AZ91D magnesium alloy. *Prog Org Coat* 63:13–17
- Tiringer U, Milošev I, Durán A, Castro Y (2018) Hybrid sol–gel coatings based on GPTMS/TEOS containing colloidal SiO<sub>2</sub> and cerium nitrate for increasing corrosion protection of aluminium alloy 7075-T6. *J Sol–gel Sci Technol* 85:546–557
- Li LJ, He JX, Lei JL, Xu WT, Jing X, Ou XT, Wu SM, Li NB, Zhang ST (2015) A sol-bath-gel approach to prepare hybrid coating for corrosion protection of aluminum alloy. *Surf Coat Technol* 279:72–78
- Mrad M, Ben Amor Y, Dhouibi L, Montemor MF (2018) Effect of AA2024-T3 surface pretreatment on the physicochemical properties and the anticorrosion performance of poly( $\gamma$ -glycidoxypolytrimethoxysilane) sol–gel coating. *Surf Interface Anal* 50:335–345
- Sonmez S, Aksakal B, Dikici B (2012) Corrosion protection of AA6061-T4 alloy by sol–gel derived micro and nano-scale hydroxyapatite (HA) coating. *J Sol–gel Sci Technol* 63:510–518
- Yu F, Akid R (2017) Corrosion protection of AA2024-T3 alloy by modified hybrid titania-containing sol–gel coatings. *Prog Org Coat* 102:120–129
- Peres RN, Cardoso ESF, Montemor MF, de Melo HG, Benedetti AV, Suegama PH (2016) Influence of the addition of SiO<sub>2</sub> nanoparticles to a hybrid coating applied on an AZ31 alloy for early corrosion protection. *Surf Coat Technol* 303:372–384
- Barajas-Ledesma E, García-Benjume ML, Espitia-Cabrera I, Bravo-Patiño A, Espinoza-Beltrán FJ, Mostaghimi J, Contreras-García ME (2010) Photocatalytic activity of Al<sub>2</sub>O<sub>3</sub>-doped TiO<sub>2</sub> thin films activated with visible light on the bacteria *Escherichia coli*. *Mat Sci Eng B* 174:74–79
- Huo KF, Gao B, Fu JJ, Zhao LZ, Chu PK (2014) Fabrication, modification, and biomedical applications of anodized TiO<sub>2</sub> nanotube arrays. *RSC Adv* 4:17300–17324
- Masudy-Panah S, Eugene YJK, Khiavi ND, Katal R, Gong X (2018) Aluminum-incorporated p-CuO/n-ZnO photocathode coated with nanocrystal-engineered TiO<sub>2</sub> protective layer for photoelectrochemical water splitting and hydrogen generation. *J Mater Chem A* 6:11951–11965
- Zhou MJ, Zeng ZO, Zhong L (2009) Energy storage ability and anti-corrosion protection properties of TiO<sub>2</sub>-SnO<sub>2</sub> system. *Mater Corros* 61:324–327
- Shi QW, Huang WX, Zhang YB, Zhang Y, Xu YJ, Guo G (2011) Curing of polyester powder coating modified with rutile nano-sized titanium dioxide studied by DSC and real-time FT-IR. *J Therm Anal Calorim* 108:1243–1249
- Wen F, Chen YQ, Cao Y, Lin SW (2011) Technical and structure study of coprecipitation method for nano-titanium dioxide. *Adv Mater* 418–420:827–830
- Niknahad M, Mannari V (2016) Corrosion protection of aluminum alloy substrate with nano-silica reinforced organic-inorganic hybrid coatings. *J Coat Technol Res* 13:1035–1046
- Cui XK, Zhu GY, Pan YF, Shao Q, Zhao C, Dong MM, Zhang Y, Guo ZH (2018) Polydimethylsiloxane-titania nanocomposite

- coating: Fabrication and corrosion resistance. *Polymer* 138:203–210
38. Song YC, Hasegawa Y, Yang SJ, Sato M (1988) Ceramic fibres from polymer precursor containing Si-O-Ti bonds. *J Mater Sci* 23:1911–1920
  39. Bera S, Rout TK, Udayabhanu G, Narayan R (2015) Comparative study of corrosion protection of sol-gel coatings with different organic functionality on Al-2024 substrate. *Prog Org Coat* 88:293–303
  40. Hegde S, Prabhu KN (2008) Modification of eutectic silicon in Al-Si alloys. *J Mater Sci* 43:3009–3027
  41. Abu-Dheir N, Khraisheh M, Saito K, Male A (2005) Silicon morphology modification in the eutectic Al-Si alloy using mechanical mold vibration. *Mat Sci Eng A* 393:109–117
  42. Xu CL, Jiang QC (2006) Morphologies of primary silicon in hypereutectic Al-Si alloys with melt overheating temperature and cooling rate. *Mat Sci Eng A* 437:451–455
  43. Xiang TF, Zheng SL, Zhang M, Sadig HR, Li C (2018) Bioinspired slippery zinc phosphate coating for sustainable corrosion protection. *ACS Sustain Chem Eng* 6:10960–10968
  44. Luo XH, Yuan S, Pan XY, Zhang CX, Du S, Liu YL (2017) Synthesis and enhanced corrosion protection performance of reduced graphene oxide nanosheet/ZnAl layered double hydroxide composite films by hydrothermal continuous flow method. *ACS Appl Mater Inter* 9:18263–18275
  45. Ye YW, Liu ZY, Liu W, Zhang DW, Zhao HC, Wang LP, Li XG (2018) Superhydrophobic oligoaniline-containing electroactive silica coating as pre-process coating for corrosion protection of carbon steel. *Chem Eng J* 348:940–951
  46. Yang LH, Wan YX, Qin ZL, Xu QJ, Min YL (2018) Fabrication and corrosion resistance of a graphene-tin oxide composite film on aluminium alloy 6061. *Corros Sci* 130:85–94
  47. Pu SM, Chen MY, Chen YQ, Zhang WT, Soliman H, Qu A, Liu QJ, Tang X, Huang N, Wan GJ (2018) Zirconium ions integrated in 1-hydroxyethylidene-1,1-diphosphonic acid (HEDP) as a metalorganic-like complex coating on biodegradable magnesium for corrosion control. *Corros Sci* 144:277–287
  48. Basu BJ, Srinivasan A, Manasa J, Grips VKW (2012) Improved corrosion protection of aluminium alloy AA2024 by sol-gel hybrid coatings after surface pretreatment by silanisation. *Surf Eng* 28:294–299
  49. Xiang TF, Ding SB, Li C, Zheng SL, Hu W, Wang J, Liu PJ (2017) Effect of current density on wettability and corrosion resistance of superhydrophobic nickel coating deposited on low carbon steel. *Mater Des* 114:65–72
  50. Akbari E, Di Franco F, Ceraolo P, Raeissi K, Santamaria M, Hakimizad A (2018) Electrochemically-induced TiO<sub>2</sub> incorporation for enhancing corrosion and tribocorrosion resistance of PEO coating on 7075 Al alloy. *Corros Sci* 143:314–328